JOURNAL OF MATERIALS SCIENCE **39** (2004) 4593–4603

Modelling of foam degradation in lost foam casting process

S. H. M. MIRBAGHERI
Department of Materials Science and Engineering, Sharif University of Technology, P.O. Box 11365-9466, Tehran, Iran; Department of Materials Science and Technology, Imperial College, SW7 2BP, London, UK
E-mail: Mohamad@mehr.sharif.edu

J. R. SILK
Department of Materials Science and Technology, Imperial College, SW7 2BP, London, UK

P. DAVAMI
Department of Materials Science and Engineering, Sharif University of Technology, P.O. Box 11365-9466, Tehran, Iran

In this investigation a new model was developed to calculate gas pressure at the melt/foam interface (Gap) resulting from foam degradation during mould filling in the lost foam casting (LFC) process. Different aspects of the process, such as foam degradation, gas elimination, transient mass, heat transfer, and permeability of the refractory coating were incorporated into this model. A computational fluid dynamic (CFD) code was developed based on the numerical technique of the SOLution Algorithm-Volume of Fluid (SOLA-VOF) utilizing model, for the simulation and prediction of the fluid flow in the LFC process. In order to verify the computational results of the simulation, a thin plate of grey iron was poured into a transparent foam mould. The mould filling process was recorded using a 16 mm high-speed camera. Images were analysed frame by frame, in order to measuring foam depolymerization rate and the gap volume during mould filling. Comparison between the experimental method and the simulation results, for the LFC filling sequence, has shown a good agreement.

Nomenclatures

C_p	Heat capacity
e	Coating thickness
F	Fraction of volume
f	Fraction of phase
g	Gravity acceleration
ΔH_f	Heat transformation
k	Thermal conductivity
K_{FGC}	Factor of foam gas capacity
P	Pressure
P_{gap}	Gap pressure
P_s	Surface pressure
P_{Int}	Initial pressure
P_{cell}	Cell pressure
P_N	Neighbour cell pressure
q	Heat flux
R_{co}	Factor of coating permeability
T	Temperature
t	Time
V_{gap}	Volume of gap
V_{gas}	Volume of gas
u	Speed in x
v	Speed in y
w	Speed in z
ρ	Density
ω	Relaxation factor
η	Interpolation factor surface
θ	Partial treatment
ν	Kinematics viscosity
Subscript (L)	Liquid
Subscript (S)	Solid

1. Introduction

In the LFC process, the pattern is usually made of expandable poly styrene (EPS) foam, which can be either moulded or hand formed to the exact shape of the casting. A gating system, also made of foam, and is attached using a suitable adhesive. The entire pattern is then coated with a refractory wash and allowed to dry. The pattern is placed into a flask, and is surrounded by clean, unbounded sand, which is compacted by vibration to give it strength. As the molten metal is poured into the flask, the metal replaces the pattern by melting, vaporisation, or foam degradation. Once the metal has solidified, the flask is emptied and the casting is cleaned. The use of a foam pattern increases dimensional accuracy, and giving improved casting quality, compared to conventional casting [1].

LFC is a much more complicated process both physically and chemically aspects rather than traditional sand casting. Many physical and chemical processes, such as heat and mass transfer, fluid flow, chemical reactions, solidification, EPS degradation, etc. are involved in this casting technique. In addition, these phenomena occur within a very short period of time during the mould filling process. It was observed that when the metal was poured, the polystyrene pattern began to decompose immediately and a gas gap was observed between the molten metal and the solid foam. This caused, an increase in the pressure within the gap (metal/foam interface) and, by altering the molten metal flows during mould filling; it has a decisive influence on the final casting quality [2]. Therefore the gas pressure due to decomposition of the EPS pattern during mould filling, is very important for designing a gating system and eliminating defects, such as cold shut, impurity and gas entrapment, and also reduction permeability of interdendritic liquid [3, 4]. It will influence the temperature distribution of liquid metal in the mould cavity and the solidification sequence. Many researchers of the LFC process have been concerned with the elimination of this degradation foam, which is a potential defect source [5–7]. Some researchers have tried to measure the backpressure inside the mould as the metal front advances. They have reported different values of gas pressure and mould filling velocity for low and high melting point alloys [8, 9].

The fluid flow phenomenon during filling of the LFC is basically a transient flow problem with the metal/foam interface. The mechanism of foam removal is governed by the rate of heat exchange between metal and foam, which in turn is defined by a heat transfer coefficient and the gaseous foam pressure between the gap of the metal and solid foam. It is difficult to measure and model the metal/foam heat coefficient directly, particularly for high melting point metals. Due to the complexity of the mathematical modelling of the LFC process, most studies have been experimental in nature, although some semi-empirical formulations regarding the fluid flow and gaseous pressures generated from foam pattern degradation have been reported. The attempts on the mathematical modelling of LFC were scarce and highly limited to a few oversimplified calculations [10].

Ohnaka developed an algorithm, which considered the backpressure change due to the foam pattern degradation in the Full Mould process [11]. Tsai, Sun, and Abayarathna used finite element method (FEM) for simulating the effect of backpressure in the LFC process [6]. The Flow Science Institute developed a finite difference code, called FLOW3D, to simulate mould-filling phenomena such as lost foam, investment, etc. [12]. Davami and Mirbagheri modified the *Advanced* solution algorithm (ASOLA-VOF) technique for the LFC via global interpolation between new and old time steps, using a shape function. They developed a 2D-CFD code for simulating the EPS casting; called SUTCAST [13, 14] Wang *et al*. modified the existing computer program for simulation of a conventional sand casting to simulate the fluid flow and heat transfer during mould filling and the ensuing solidification for the LFC processes, in an arbitrary 3-D geometry [15]. Liu *et al*. developed a simple 1-D mathematical model, which predicted the molten metal front velocity and backpressure of the decomposed gasses for the LFC process [10].

With regards to the published research, further study is still required into the effect of backpressure on the filling stage in the LFC process. In this study, the SOLA-VOF technique was modified to account for the backpressure effect during the LFC process. The proposed model is capable of considering the effect of various parameters such as, burning foam rate, gas foam pressure, permeability and thickness of refractory coating and foam density. The model was then tested for a lost foam benchmark using cast iron.

2. Mathmatical modelling

2.1. Physical model for foam degradation

In order to observe, the gap volume, size and morphology of the gap between the metal front and foam pattern, as shown in Fig. 1, a flask was designed and built to permit direct observation of the foam degradation through a Pyrex window, with an overlaid wire netting, during mould filling. The wire netting was used for calculating the gap volume and preventing fragmentation of the glass windows. The main scope for the modelling of foam degradation is calculating gas pressure due to foam burning at the metal/foam interface (gap space). This gas pressure increase is called *backpressure*, which has a decisive influence on the liquid metal flow during mould filling. Therefore, the main problem in the backpressure modelling is how to measure the gap volume and the released gas from this volume at each small time step during mould filling.

If the pouring time is divided into small time steps, dependent on the pouring time, it could be considered as a quasi-steady state. Thus, the ideal gas law could be modified for measuring the pressure in the gas gap. Equation 1, for a constant temperature, is the same as the ideal gas law when all constant factors are equal to one.

$$(aP_1)^{b}(cV_1)^{d} = (a'P_2)^{b'}(c'V_2)^{d'} \tag{1}$$

In order to the obtain the gap pressure in the LFC process, the following sequences have to be followed:

(i) Measuring the mass of burnt foam in each time step or gap volume.
(ii) Measuring the volume of released gas from mass determined in step (i).
(iii) Measuring the gap pressure, considering the permeability of the refractory coating.

In the first step, the volume of the gap (V_{gap}) is measured by a new method. In this method a sheet of wire netting was put in front of Pyrex window. As shown in Fig. 1, the V_{gap} is determined by the summation of the mesh areas of the wire netting, between the interfaces of the foam and melt multiplied by the thickness of the foam pattern. This is achieved by analysis of

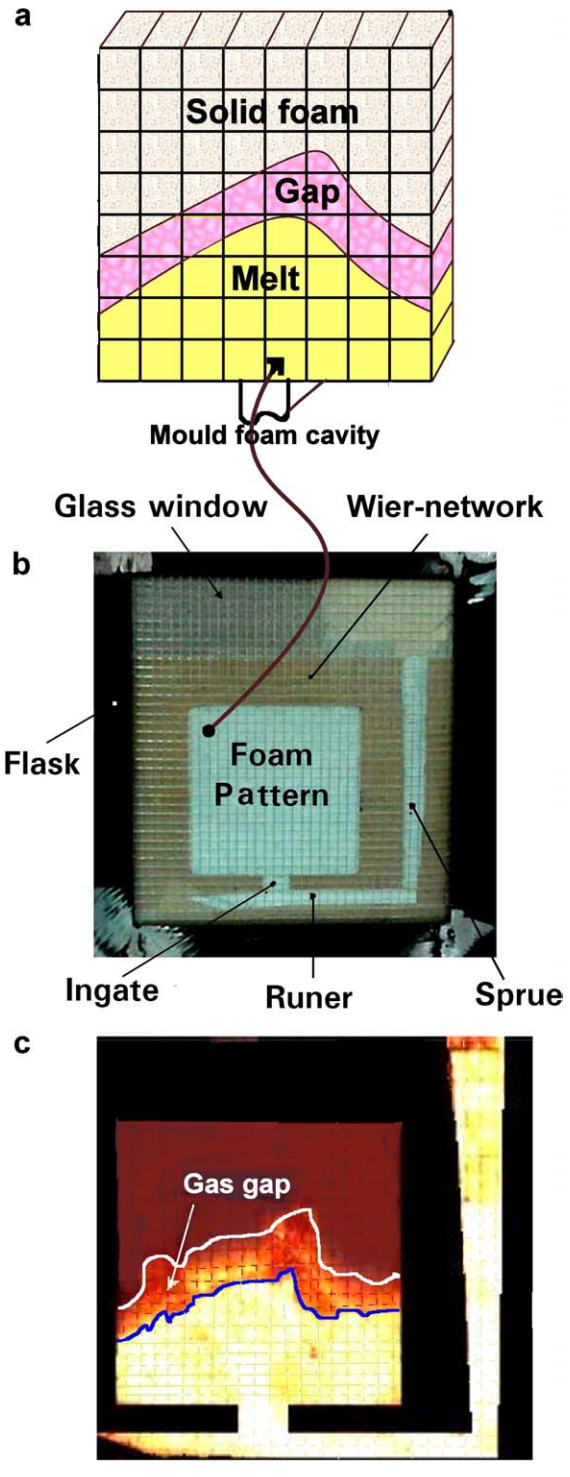

Figure 1 Desing of the flask with one transparent face for measuring the gas gap volume with a high-speed camera. (a) Schematic of gap between solid foam and melt, (b) Flask before casting, and (c) Flask during casting.

the frame-by-frame images from a 16 mm high-speed camera, during mould filling. Fig. 2 shows that the V_{gap} obtained by this method is between 4.0–4.5 times the volume of molten poured into the cavity mould (V_M), at each time step. This ratio called 'Gap Height' coefficient (k_{gh}), and is dependent on the characteristics of refractory coating and molten metal. Foe example, k_{gh} is between 4.0–4.5 for high melting point alloys, and 2.0–3.0 for low melting point alloys [14].

In the second step, by burning a certain amount of foam, the volume of the gas released per unit mass

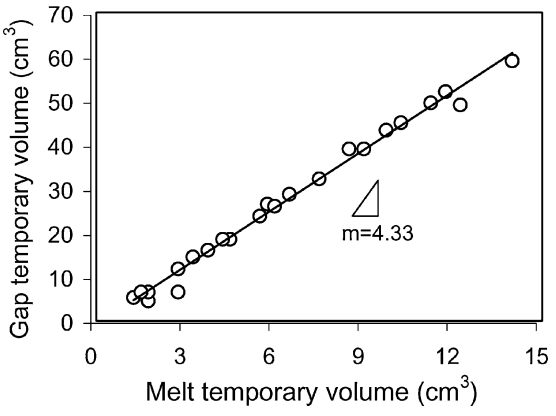

Figure 2 Measuring the melt and gap volume in each of the two sequences using photograph frames during the mould filling.

of foam, e.g., Foam Gasified Capacity (k_{FGC}), can be measured. The k_{FGC} is a function of the density, foam type and degradation temperature. For example, k_{FGC} for polystyrene foam with density of 0.014 gr/cc is 300-cc/gr (see Section 4) Therefore the gas volume produced by foam degradation (V_{gas}) in each time step (t) of total filling time was equal to $k_{FGC} \times (V_{gap} + V_M) \times$(foam density). This large amount of gas accumulates between interface solid foam and molten.

In the final step, the gap pressure (P_{gap}) in each small time step was obtained on a quasi-static balance of the gas volume due to foam degradation, and the amount of gas escaping through the pores of refractory coating.

Experimental results using polystyrene foam with various densities were used for calibrating the ideal gas law (see Section 4). These results show that in Equation 1, for liquid grey iron; $b = b' = 1$, $d = d' = 2$, a/a', c/c' are dependent on coating permeability, the value of the k_{FGC} coefficient, and $V_{gap} = V_1$, $V_{gas} = V_2$. Thus the ideal gas law could be modified for measuring the temporary gap pressure as follows:

$$\bar{P}_{gap} = P_{Int} V_{gas}^2 \left(R_{co}^{1.20} e^{m} \bar{V}_{gap}\right)^{-2} \quad \text{if} \quad 1000 < T \leq 1500^{\circ}\text{C} \qquad (2)$$

where P_{gap} is the temporary gap pressure, P_{Int} the initial pressure step, k_{FGC} the FGC coefficient, e the ratio thickness of the coating to the minimum pattern thickness, and R_{co} is the hot permeability of the refractory coating. If the coating thickness is greater than 1.0 mm, $m = 0.51$, and if the coating thickness is equal to or less than 1.0 mm, $m = 1.2$.

From the above discussion, it can be seen that P_{gap} is dependent on the V_{gap}, which in turn, is obtained from the results of the analysis of the high-speed camera images. Therefore, in next step instead of using the photography method for measuring the gap volume, a fluid flow simulation code that has already been developed is utilized [16]. In other words according to experimental results, the volume of burnt foam is equal to the temporary volume of liquid flown into the cavity mould multiplied by the k_{gh} coefficient. Thus, having the volume of metal enter the mould cavity in each time step by utilizing the CFD code, the volume of burnt foam can be calculated by the k_{gh} coefficient as well as P_{gap}

by Equation 2. Hence, the P_{gap} is substituted for the pressure term of the Navier–Stokes equations, for simulating the effect of backpressure on the behaviour of fluid flow, as mentioned in the next section.

2.2. Mathematical model of the fluid flow

2.2.1. The governing equations

(a) *The free surface function*: The most common method used to describe free surfaces is the VOF method. This method enables the tracking of the free surface transition with arbitrary topology and deformation, according to:

$$\frac{\partial F}{\partial t} + \nabla \cdot \vec{V} F = 0 \tag{3}$$

In the VOF technique, a function $F(x, y, z, t)$ is defined which is the fractional volume of the control element occupied by fluid. F has a range from zero to unity; the cell having F values between zero and one ($0 < F < 1$) represents the free surface. $F = 0$ indicates that the cell contains no fluid and $F = 1$ corresponds to a cell full of fluid. The position of the interface, curvature and normal direction to the free surface can all be determined from the derivatives of F values in a control volume [17].

(b) *The momentum transport equation*:

$$\rho \frac{D\vec{V}}{Dt} = -\nabla P + \rho \vec{g} + \mu \nabla^2 \vec{V} \tag{4}$$

(c) *The heat transfer equation*:

$$\rho C_p \frac{\partial T}{\partial t} = -\rho C_p \vec{V} \cdot \nabla T + \nabla \cdot \vec{q} \tag{5}$$

$$\vec{q} = -\left(k \frac{\partial T}{\partial x} \hat{i} + k \frac{\partial T}{\partial y} \hat{j} + k \frac{\partial T}{\partial z} \hat{k} \right) \tag{6}$$

(d) *The continuity equations*:

$$\frac{\rho_L - \rho_s}{\rho} \left[\frac{\partial f_L}{\partial t} + (\vec{V}) \cdot \nabla f_L \right] + \nabla \cdot (\vec{V}) = 0 \tag{7}$$

$$f_L + f_s = 1, \quad \text{and} \quad \rho = \rho_s f_s + \rho_l f_l$$

(e) *The decomposition function of foam:* The amount of gas pressure due to foam degradation on the free surface (gap) in each time step is calculated from Equation 2. It should be noted that the validity of Equation 2 demands a very short time, which should be defined according to the pouring time. As mentioned in Section 2.1, temporary gap volume is a linear function from temporary liquid volume, which enters into the mould cavity. This volume can be calculated by a numerical method too. In order to for a 3D cell in the free surface of the liquid, the volume of the fluid fluxes across the faces of the cell and its location should be calculated by the Donor-Acceptor flux approximation. At each face of the 3D computing cell, the two cells immediately adjacent to the interface are distinguished, one becoming a Donor cell and the other an Acceptor cell, and cell quantities are given the subscripts D and A, respectively, e.g., F_D and F_A. Therefore a 3D cell has six faces and six neighbouring cells that each adjacent cell has label F_D or F_A, and six faces will have a label $F_{AD.}$ Fluid volume fluxes across the faces of the 3D cells are obtained based on Equation 3, as follows. Further information can be found in the reference [14, 16, 18, 19]:

$$\begin{aligned} F^{n+1}_{i,j,k} - F^{n}_{i,j,k} &= -\overline{\delta t} \left\{ \frac{1}{\triangle x} \left[U^{n+1}_{i+1,j,k} F_{i+1,j,k} - U^{n+1}_{i-1,j,k} F_{i-1,j,k} \right] \right. \\ &+ \frac{1}{\triangle y} \left[V^{n+1}_{i,j+1,k} F_{i,j+1,k} - V^{n+1}_{ij-1,k} F_{i,j-1,k} \right] \\ &\left. + \frac{1}{\triangle Z} \left[W^{n+1}_{i,j,k+1} F_{i,j,k+1} - W^{n+1}_{i,j,k-1} F_{i,j,k-1} \right] \right\} \end{aligned} \tag{8}$$

For example, the first term of the right-hand side of Equation 8 is calculated as follows:

$$\begin{aligned} \delta F^{R+}_x &= F_{AD} U^{n+1}_{i+1,j,k} \overline{\delta t} = \mathrm{sgn}\left[U^{n+1}_{i+1,j,k} \right] \mathrm{MIN}\left[F_{AD} \right. \\ &\left. \times \left| \forall^{R+}_x \right| + \mathrm{CFXR}^+, F_D \triangle X_D \right] \end{aligned} \tag{8a}$$

$$\begin{aligned} \mathrm{CFXR}^+ &= \mathrm{MAX}\left[(1.0 - F_{AD}) \left| \forall^{R+}_x \right| - (0.1 - F_D) \right. \\ &\left. \times \triangle X_D, 0.0 \right]; \quad \forall^{R+}_x = U^{n+1}_{i+1,j,k} \delta t \end{aligned} \tag{8b}$$

The MIN term in Equation 8a prevents fluxing more fluid per unit area than the donor cell contains, while the MAX term in Equation 8b prevents fluxing of more void per unit area than the donors cell contains. A similar method is used to calculate other cell faces. However, to determine whether F_{AD} is F_D or F_A, the labelling is accomplished by means of the algebraic sign of the fluid velocity normal to the interface; the donor cell is always upstream, and the acceptor cell is down-stream, with respect to the interface [17, 18]. The left-hand Equation 8 gives the volume fraction of the net liquid amount, which flew into the computational cell (*i, j, k*) in the time step $\overline{\delta t} = 1/2(\delta t^n + \delta t^{n+1})$. Thus, the molten volume flown into the mould cavity can be calculated from the difference of the molten level (free surface) in two successive time steps, according to:

$$\begin{aligned} V_{gap} &= k_{gh} \triangle V_{M-F} = k_{gh} \sum \left(F^{n+1}_{i,j,k} - F^{n}_{i,j,k} \right) \\ &\times \triangle x \triangle y \triangle z \quad \text{if } 0 < F_{i,j,k} < 1 \end{aligned} \tag{9}$$

Therefore, knowing the melt volume that has entered the mould cavity, the volume of burnt foam can be calculated using Equation 9. By substituting this value into Equation 2, P_{gas} (due to the foam degradation) can be obtained.

2.2.2. Numerical computation technique

The main purpose of the simulation in the LFC process is to calculate the velocity profile, and the temperature field due to the backpressure effect during mould

filling. Then the finite difference approximation method can be considered in four steps: (i) System discreatization. (ii) Finite difference approximations form of governing equations. (iii) Determination of fluid volume fluxes across the faces of the elements and free surface location by Donor-Acceptor flux approximation, and also calculation of the pressure and the volume of the gap between solid foam and melt front. (iv) Semi-explicit solution of the finite difference approximation of momentum and heat transfer equations for calculating velocity profile and temperature field in the system

The computation procedures are as follows:

(1) Initial conditions are set, including mesh size generation, initiating arrays, the control parameter set-up and physical-thermal property parameters.

(2) The calculation is made for each time step by FDM. The basic procedure of advancing a solution through one increment in time, δt, consists of several steps:

(i) Semi-explicit SOLA-VOF approximations of Equations 7, 8 and 9 are used to compute the first guess for a new time-level velocities using the initial conditions or previous time-level values for all advective, pressure, and viscous accelerations.

(ii) To satisfy the continuity equation, Equation 10, pressures are iteratively adjusted in each cell and the velocity changes, induced by each pressure change, δP, are added to the velocities computed in step (1). The δP for *full* (liquid) and *surface* (gas gap) cell is calculated from [16, 17]:

$$\delta P_{\mathrm{i,j,k}} = -D_{\mathrm{i,j,k}}\left[\frac{\partial D_{\mathrm{i,j,k}}}{\partial P}\right]^{-1} = D_{\mathrm{i,j,k}}\left[\frac{\delta t}{\rho}\left(\frac{1}{\triangle x}\left(\frac{1}{\triangle x_{\mathrm{right}}}+\frac{1}{\triangle x_{\mathrm{left}}}\right)+\frac{1}{\triangle y}\left(\frac{1}{\triangle y_{\mathrm{top}}}+\frac{1}{\triangle y_{\mathrm{botom}}}\right)+\frac{1}{\triangle y}\left(\frac{1}{\triangle z_{\mathrm{front}}}+\frac{1}{\triangle z_{\mathrm{back}}}\right)\right)\right]^{-1} \quad \text{for full cell} \quad (10)$$

$$\delta P_{\mathrm{i,j,k}} = (1-\eta)P_{\mathrm{N}} + \eta P_{\mathrm{S}} - P_{\mathrm{i,j,k}} \quad \text{for surface cell} \quad (11)$$

where P_{s} is the gas pressure, due to foam degradation that acts on the free surface e.g., P_{gap}, and $\eta = \mathrm{d_c}/d$, as shown in Fig. 3, is the ratio of the distance between the cell centres and the distance between the free surface and the centre of the interpolation cell.

(iii) The F function defining fluid regions should be updated to give the new fluid configuration.

(iv) Finally, the temperature in each cell is calculated by means of Equation 5, and then the solid fraction or liquid fraction of metal in each cell is determined.

(3) Repeating the above steps will advance a solution through any desired time interval. At each step, suitable boundary conditions must be imposed at all meshes and free surface boundaries. When the fraction of liquid in any cell falls bellows a certain value ($f_{\mathrm{L}} < 0.35$), that cell is treated as a solid obstacle and motionless [16, 20]. The flow chart of SOLA_VOF solution procedures is given in Fig. 4.

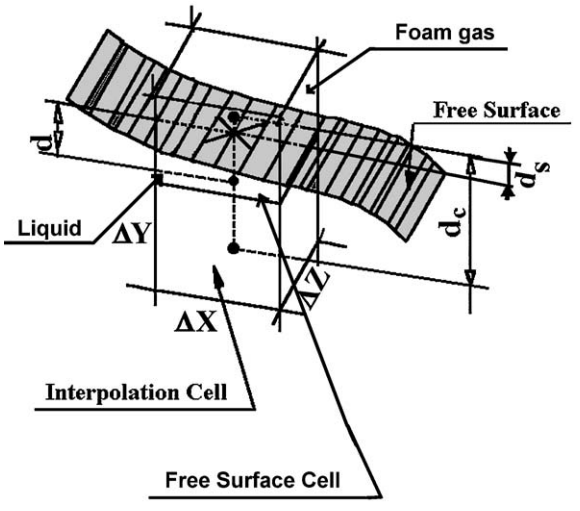

Figure 3 Schematic of the interpolation and free surface cell, in three-dimensional space.

3. Experimental procedure

In order to observe the fluid dynamics of mould filling in the LFC process, as shown in Fig. 1; a flask was designed and built for direct observation of the sequence and burning of foam, through a Pyrex window, with overlay wire netting. The wire-netting mesh was used to calculate the gap volume and to prevent fragmentation of the glass windows. The geometry, dimensions, gating system and schematic of experimental equipment are shown in Fig. 5 for a vertical benchmark plate. The foam pattern used in these experiments was made using the EPS bead with grade *C* (e.g., sieve size 36–60, AFS 38 gfn, raw size 0.508–0.254 mm, density = 0.014 gr/cm^3)[1]. The foam pattern and gating systems were then dipped (except one face of the foam plate) in a refractory slurry or coating, removed and rotated slowly to insure the coating covered all the foam surfaces, and allowed to dry. The foam pattern was assembled on a Pyrex sheet with a non-coated face and then placed in the flask, which had already been assembled on vibrating apparatus while it was filled with sand. In order to determine the gas pressure of degradation foam, two bronze tubes with 2 mm in diameter and 250 mm in length were attached to two sides mould. The ends of the tubes were connected to gas pressure transducers (GPT), which had a maximum, rang 20,000 ± (10) Pa, as shown in Fig. 5.

Also two set thermocouples were inserted into the foam and sand (attached to coating) to record the temperature of the mould cavity and coating. The thermocouples were located in the centre point of the benchmark plate and sand mould, just under the refractory coating. The use of thermocouples ensured no premature non-solidification during mould filling.

Both the temperature and pressure data were downloaded to a computer utilizing a PLC-32bit card of

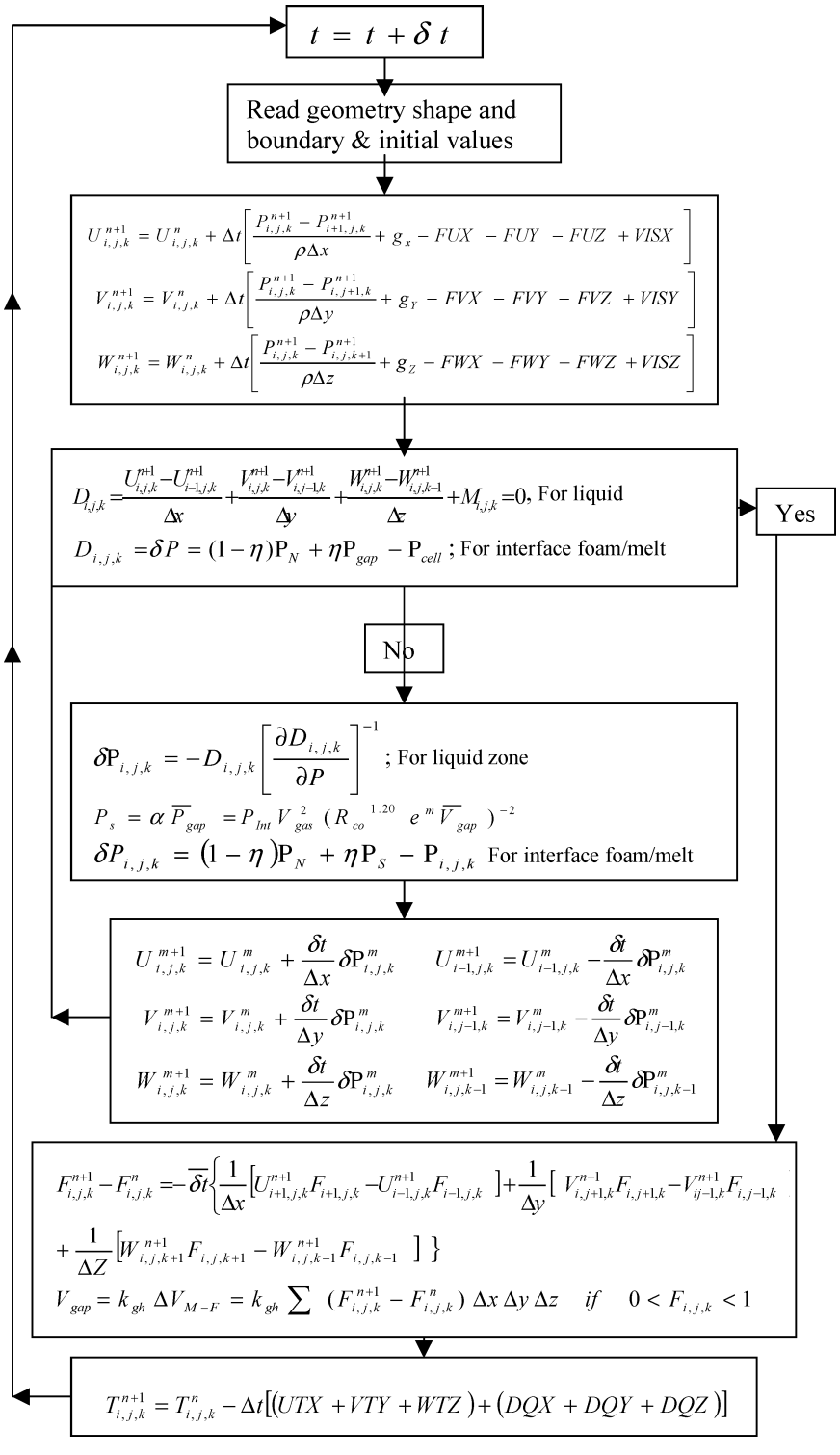

Figure 4 Algorithm of modified SOLA-VOF method for the determination of the backpressure.

10 kHz, 12 channels, HG818L-Advantech. Each measurement of temperature and pressures was duplicated for reliability purposes.

A high frequency induction furnace was used to melt grey iron with a chemical composition of: $C = 3.8\%$, Si $= 2.2.5\%$, Mn $= 0.75\%$, $P = 0.11\%$, $S = 0.22\%$. Finally, the molten metal was poured at a temperature of 1350°C, and the mould filling was recorded simultaneously with a 16-mm high-speed camera (64 frames/s). The pressure of the foam pyrolysis and the temperature were collected by a data acquisition system during mould filling.

4. Result and discussion

Fig. 6 shows that the metal filled the mould as quickly as the pattern degraded. A gas gap was observed between the liquid metal and foam pattern during filling. As shown in Fig. 1, the gap volume was calculated by analysis of the frame-by-frame photography images, in which the area of the wire netting meshing between the interfaces of foam/melt was summed and multiplied by the thickness of the benchmark plate. Fig. 7 shows profiles for the gap and melt volume, respectively, which were obtained by analysis of the frame-by-frame images from the16-mm high-speed camera taken every

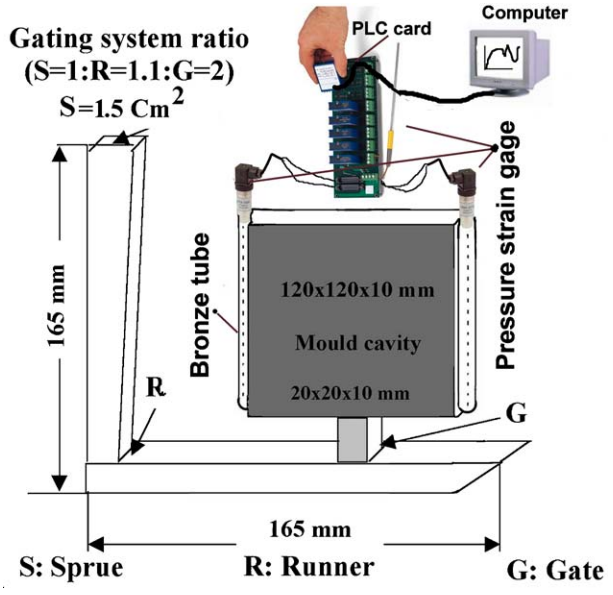

Figure 5 Installation of the pressure strain gage and the data acquisition system on the flask.

1/8 s. These frames included 24 images from the first to the final moments of the filling process. As shown in Fig. 2, the correlation between the V_M and the V_{gap} is linear, which is the slope is k_{gh}. Thus according to experimental results, the volume of the burnt foam is between 4.0–4.5 times the volumes of the cast iron liquid flown inside the mould cavity, in each time step.

Fig. 8 shows numerical and experimental profiles for the mould filling sequences. The difference in the early stages of filling is due to inclusion of the amount of melt in the gaiting system for numerical computations. As mentioned previously due to burning of the foam, the pressure in the gap is increased. This increase in pressure was transmitted to GPT and then the data was saved on a PC using a data acquisition system that was capable of plotting pressure versus time. Fig. 9 shows experimental and numerical pressure profiles during of mould filling. Once the metal front had reached the location of the bronze tube, the gas pressure inside the cavity rose rapidly to the maximum value, 4.86 kPa after 3 s. However, the pressure sharply decreased from 4.86 to 0.022 kPa at point M of curve $P - t$, as when the cavity filling was completed, suddenly Pyrex glass window fractured, and molten metal was discharged. This maximum pressure depends on the foam density and type. For example, the gas pressure of foams with a density of 0.02 gr/cm^3 is about 12.50 kPa. Fig. 10 shows the maximum gas pressure obtained from GPT for different densities of foam for grey cast iron, and is compared with data reported by other researchers [9, 21, 22]. The temperature variation in Fig. 11 shows that the temperature of the cavity and the coating increases during mould filling without any solidification. When cavity filling was completed, with the sudden fragmentation of the Pyrex glass, the thermocouples and pressure transducers could not record the rest of the solidification process. Also, in Fig. 11, for the centre point of benchmark plate, numerical temperatures results were plotted, in order to compare them with the experimental results.

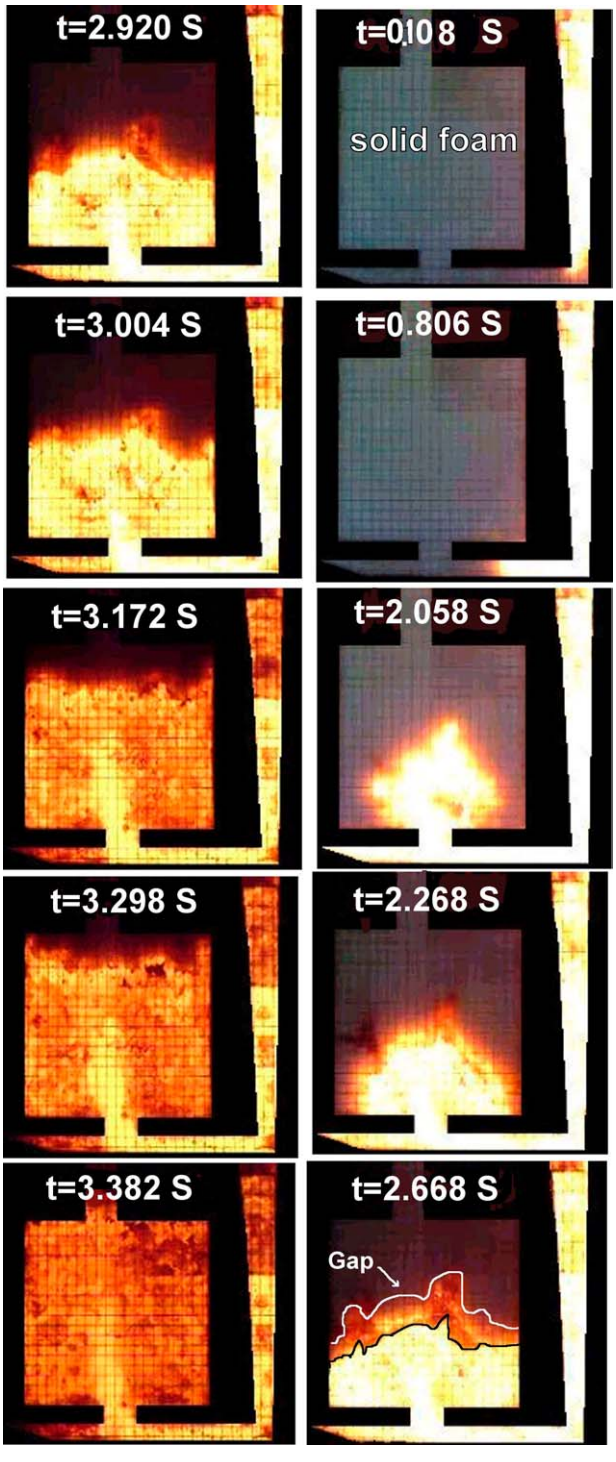

Figure 6 Photographs of the lost foam casting process. *Molten metal*: gray iron, *Mould materials*: unbounded silica sand, *Filling time*: 3.382 Sec.

Fig. 12 shows the results of the LFC simulation, based on the data in Table I, including the thermophysical properties of grey iron, meshing type and initial and boundary conditions. The predicted flow pattern, filling sequences and temperature distribution are the same as the experimental results shown in Fig. 6. The comparison between experimental results obtained from the high-speed camera (actual casting) in Fig. 6, and simulation results (virtual casting) in Fig. 12, verifies that the predicted flow patterns are comparable with the experimental results. Also, a mathematical–experimental model (Equation 6), which was developed to calculate the effect of backpressure on filling

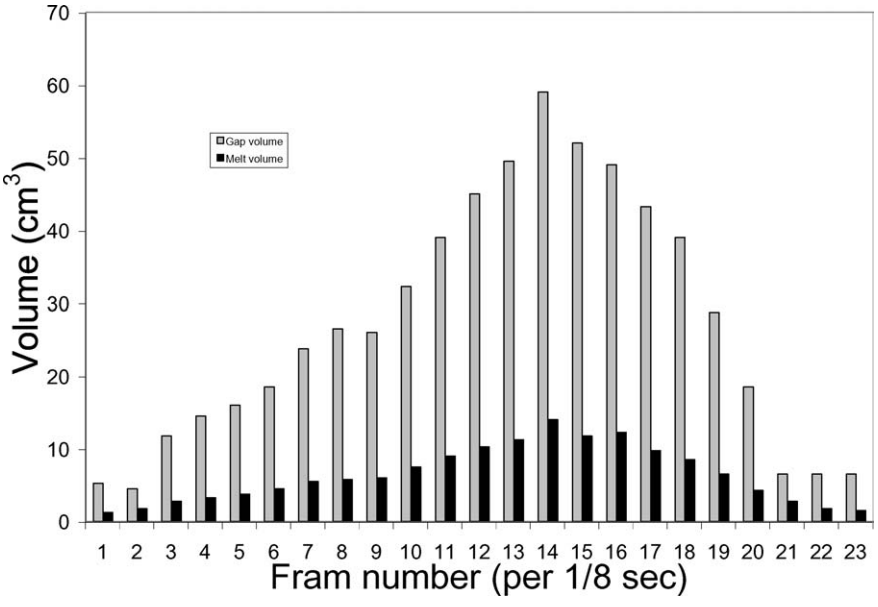

Figure 7 Measuring of the gap and melt volumes by analyzing frame-by-frame images.

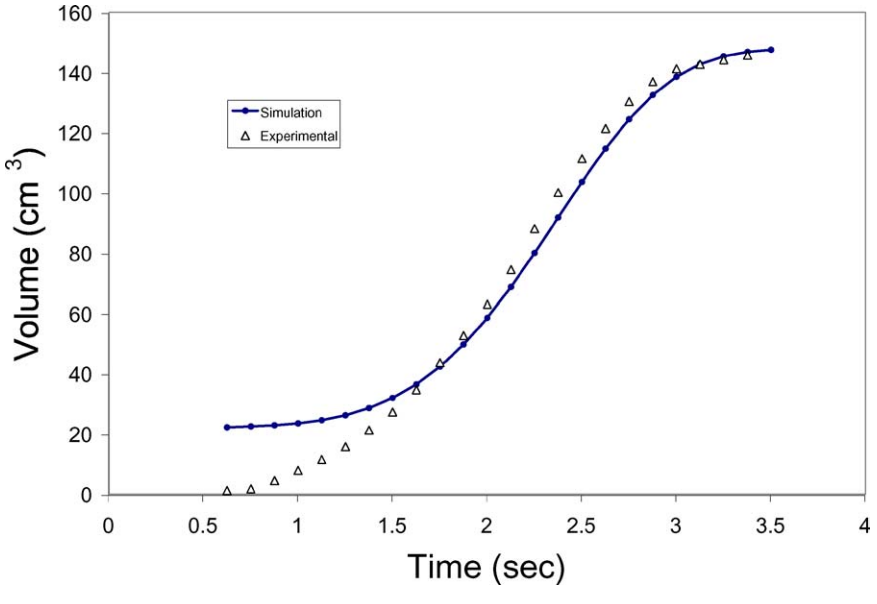

Figure 8 Profiles of filling time in a benchmark plate for both experimental and simulation methods.

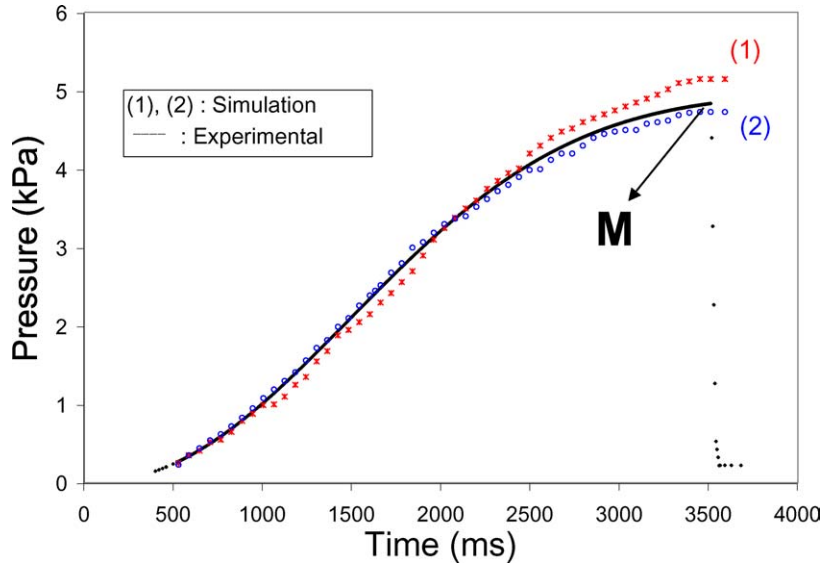

Figure 9 Changes of pressure during mould filing. (1) Simulation results with 5 × 5 mm mesh, (2) simulation results with 2 × 2 mm mesh, (•): experimental results from pressure strain gauge.

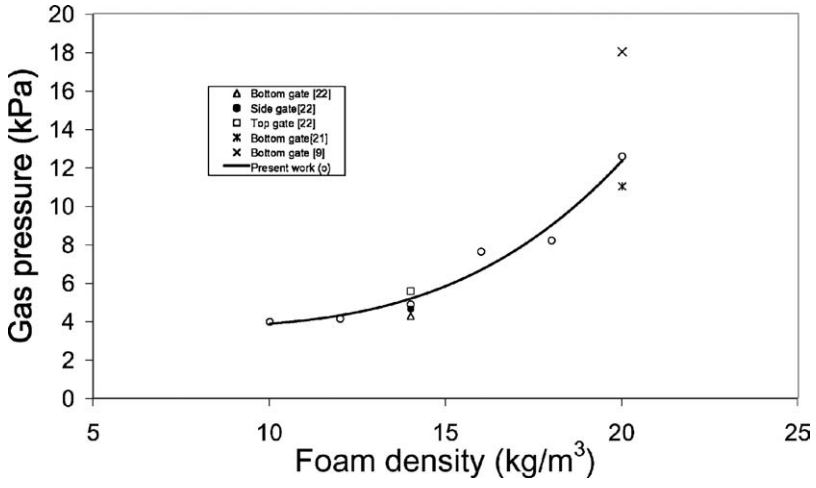

Figure 10 The foam gasified capacity is plotted as a function of foam density: (−) best fit between data (o) of present work; Δ, •, □ symbols: ref. [22]; *: ref. [21]; x: ref: [9].

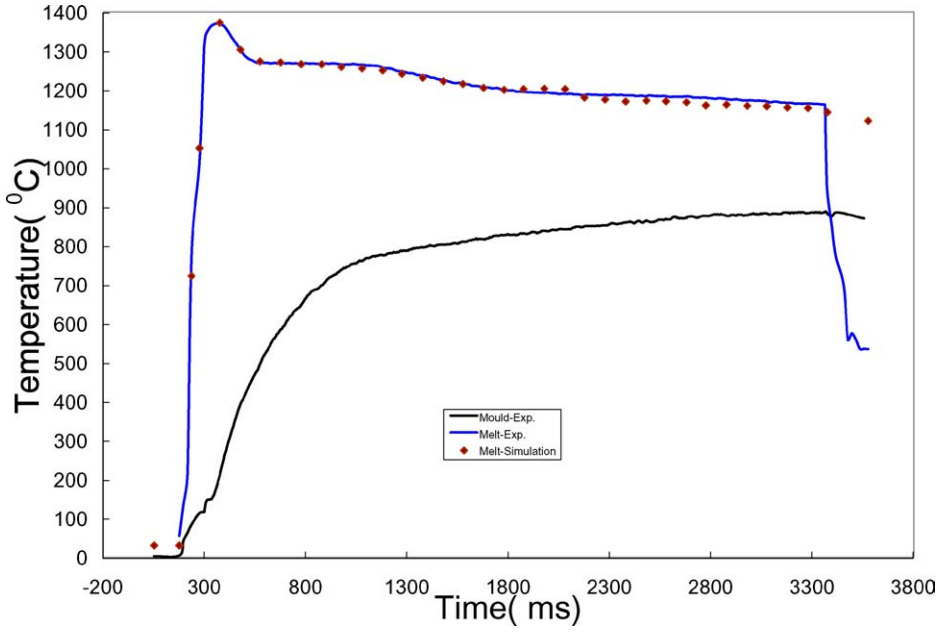

Figure 11 Profiles of temperatures in a benchmark plate, (•): simulation-melt, (1) experimental-melt and (2) experimental mould.

TABLE I Vertical plate gravity casting-simulation data

Property	Value
Material: *Cast iron* (wt)	C = 2.3, Si = 2.2, Mn = 0.75, S < 0.01, P < 0.02
Pouring temperature (°C)	1350 ± 5
Thermal conductivity (Cal/sec. cm °C)	$k_L = 0.069$, $K_s = 0.07$, $k_{sand} = 0.001$
Heat of fusion (cal/gr.)	$\Delta H_f = 49.76$
Viscosity (cm^2/sec.)	$\mu = 0.02368$
Specific heat (cal/gr. °C)	$C_p^l = 0.23$, $C_p^s = 0.21$, $C_p^{sand} = 0.23$
Density (gr./Cm^3)	$\rho_L = 7.2$, $\rho_s = 7.3$, $\rho_{Sand} = 1.61$, $\rho_{Foam} = 0.014$
Transformation temperature (°C)	$T_L = 1270 \pm 1$, $T_S = 1150 \pm 1$
Number elements of cavity	N = 7454280
Dimension elements of cavity (cm)	$\Delta x = \Delta y = \Delta z = 0.054$
CPU time for Pentium III 600 (min)	299
Boundary conditions	Wall: *free slip* Inlet: constant *pressure* = 15 mbar

behaviour, shows good agreement for high melting point alloys ($T_m > 1000$°C), confirming the accuracy of the present model.

Simulation results of the pressure due to the foam degradation for some different mesh sizes are plotted in Fig. 9. These numerical results were obtained using present code, which was developed based on the new experimental model (Equation 2). They show good agreement with the experimental results.

5. Conclusions

The computational fluid dynamics code developed in this investigation can simulate the effect of backpressure, due to the foam degradation in the LFC process, by combining a new mathematical model and the VOF method. In this model, the mould filling is controlled by the foam degradation for high melting point alloys, because during mould filling, the amount of gas released from the foam degradation must permeate the

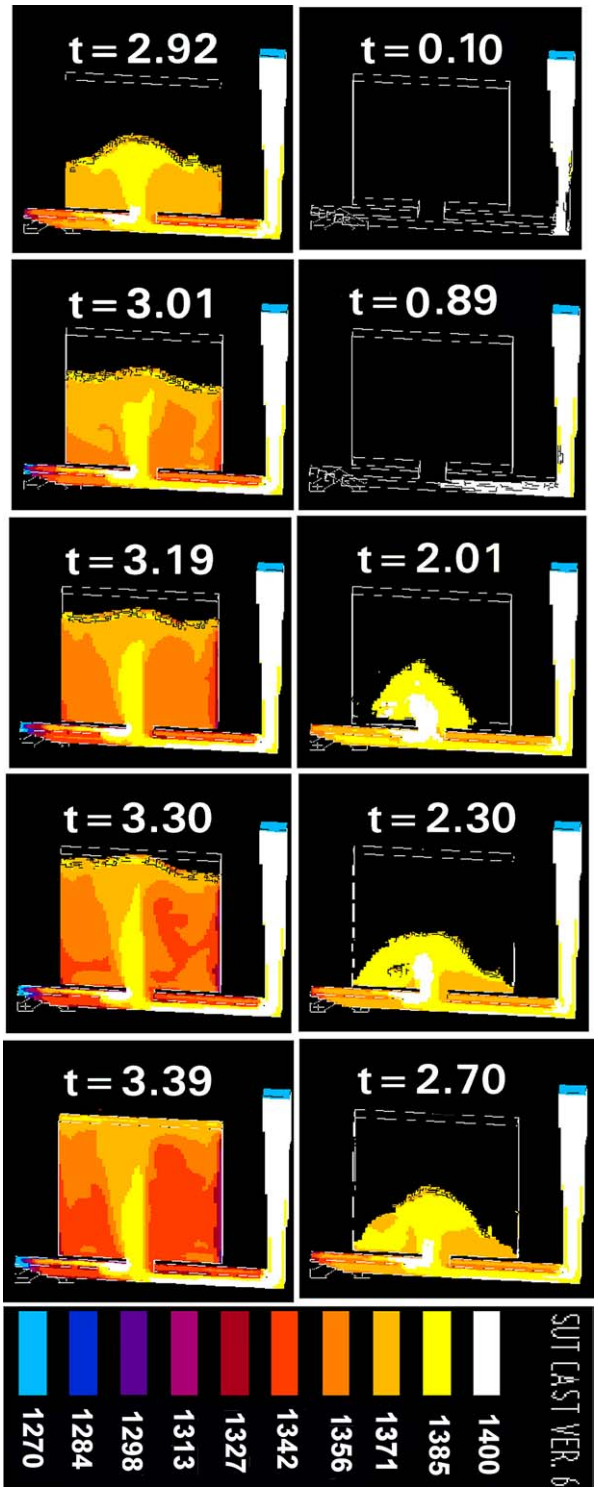

Figure 12 Simulation of mold filling in the LFC process, *Molten metal*: gray iron, *Mould materials*: unbounded silica sand, *Filling time*: 3.39 Sec

coating. Therefore, the permeability of the coating and the amount of gas evolved from the mass unit of foam are the most important factors controlling the gap pressure. Thus in the simulation of the fluid flow in the LFC process, the effect of backpressure should be considered, as this control will eliminate defects, such as porosity, gas entrapment and cold shut.

The Present code can predict the flow pattern; burn rate of the foam, the filling sequence, and the temperature distribution in the metal and mould throughout the filling period of the LFC for complex shapes. The results of this code show good agreement between simulation and experimental results and also some of the data reported in the literature.

Acknowledgments

Funding for this project was provided by the RMRC (Razi Metallurgical Research Centre). Its support is gratefully acknowledged. The authors are grateful for the research support of the Sharif University of Technology and Department of Materials at Imperial College, London.

Appendix A

(1) *The finite difference approximations for momentum transport equation*:

$$U_{i,j,k}^{n+1} = U_{i,j,k}^{n} + \Delta t\left[\frac{P_{i,j,k}^{n+1} - P_{i+1,j,k}^{n+1}}{\rho \Delta x} + g_x - \mathrm{FUX} - \mathrm{FUY} - \mathrm{FUZ} + \mathrm{VISX}\right] \quad \text{(A1)}$$

$$V_{i,j,k}^{n+1} = V_{i,j,k}^{n} + \Delta t\left[\frac{P_{i,j,k}^{n+1} - P_{i,j+1,k}^{n+1}}{\rho \Delta y} + g_y - \mathrm{FVX} - \mathrm{FVY} - \mathrm{FVZ} + \mathrm{VISY}\right] \quad \text{(A2)}$$

$$W_{i,j,k}^{n+1} = W_{i,j,k}^{n} + \Delta t\left[\frac{P_{i,j,k}^{n+1} - P_{i,j,k+1}^{n+1}}{\rho \Delta z} + g_z - \mathrm{FWX} - \mathrm{FWY} - \mathrm{FWZ} + \mathrm{VISZ}\right] \quad \text{(A3)}$$

where the superscript (n) stands for old time level, and ($n + 1$) for the new time level, and FUX, FUY, FUZ, FVX, FVY, FVZ, FWX, FWY, FWZ are advective flux terms, and VISX, VISY, VISZ are viscous flux terms. Further details can be found in references [16–19].

(2) *The finite difference approximation for heat transfer equation*:

$$T_{i,j,k}^{n+1} = T_{i,j,k}^{n} - \Delta t[(\mathrm{UTX} + \mathrm{VTY} + \mathrm{WTZ}) + (\mathrm{DQX} + \mathrm{DQY} + \mathrm{DQZ})] \quad \text{(A4)}$$

UTX, VTY and WTZ are heat convection terms, and DQX, DQY and DQZ are heat diffusion terms. In the freezing range the specific heat and liquid fraction of the mushy metal is found through *C*p method [16].

(3) *The finite difference approximation for continuity equation is*:

(i) For *full* cell ($F = 1$):

$$D_{i,j,k} = \frac{U_{i,j,k}^{n+1} - U_{i-1,j,k}^{n+1}}{\Delta x} + \frac{V_{i,j,k}^{n+1} - V_{i,j-1,k}^{n+1}}{\Delta y} + \frac{W_{i,j,k}^{n+1} - W_{i,j,k-1}^{n+1}}{\Delta z} + M_{i,j,k} = 0 \quad \text{(A5)}$$

where amount of the $M_{i,j,k}$ is equal zero in liquid zone and non-zero in mushy zone.

(ii) For *surface* cell ($0 < F < 1$): $D_{i,j,k}$ of the free surface is satisfied by setting the surface cell pressure (P_{cell}) equal to the value obtained by linear interpolation between the gap gas pressure at the free surface (P_{gap}) and the pressure inside the liquid (P_N) according to.

$$D_{i,j,k} = \hat{\delta} P = (1-\eta)P_N + \eta P_{gap} - P_{cell} \quad \text{(A6)}$$

Where:

$$\eta = \frac{d_c}{d} = \frac{d_c}{d_c - d_s} = \left(1 - \frac{d_s}{d_c}\right)^{-1}$$

$$d_s = \begin{Bmatrix} d_w(0.5 - F_{i,j,k}) & \text{if } F_{i,j,k} > 0.5S \\ d_w 0.5(1 + S - \sqrt{8SF_{i,j,k}} & \text{if } F_{i,j,k} \le 0.5S \end{Bmatrix},$$

$$S = \left|\frac{\text{slope}}{\text{scale}}\right|$$

$$d_w = \begin{cases} \Delta x & \text{if UNV of } surface = i \\ \Delta y & \text{if UNV of } surface = j \\ \Delta z & \text{if UNV of } surface = k \end{cases}$$

$$\text{slope} = \begin{cases} \text{Min}\left(\dfrac{\partial F_{yz}}{\partial z}, \dfrac{\partial F_{yx}}{\partial x}\right) & \text{if UNV of } surface = j \\ \text{Min}\left(\dfrac{\partial F_{zy}}{\partial y}, \dfrac{\partial F_{zx}}{\partial x}\right) & \text{if UNV of } surface = k \\ \text{Min}\left(\dfrac{\partial F_{xz}}{\partial z}, \dfrac{\partial F_{xy}}{\partial y}\right) & \text{if UNV of } surface = i \end{cases}$$

scale

$$= \begin{cases} \text{Max}(\Delta y/\Delta z, \Delta y/\Delta x) & \text{if UNV of } surface = j \\ \text{Max}(\Delta z/\Delta y, \Delta z/\Delta x) & \text{if UNV of } surface = k \\ \text{Max}(\Delta x/\Delta z, \Delta x/\Delta y) & \text{if UNV of } surface = i \end{cases}$$

As shown in Fig. 3, d_c, is the distance between the cell centres, d_w, the width of the surface cell, and d_s the distance from the centre of the surface cell to the fluid surface, UNV a unit normal vector of the surface and S is the surface ratio [16, 20].

References

1. R. M. MONROE, "Expendable Patterns Casting" (American Foundry-Man's Society Inc., 1992) p. 84.
2. C. H. TSENG, "A Study of the Mould Filling Parameters in the Evaporative Pattern Casting Process," Ph.D. Thesis, Missouri-Rolla University, USA, 1991.
3. Ø. NIELSEN, B. APPLAIRE and H. COMBEAU, *Metall. Mater. Trans.* A **32A** (2001) 2049.
4. A. J. DUNCAN and Q. HAN, *ibid.* B **30B** (1999) 7745.
5. Y. SUN, D. ASKELAND and H. TSAI, *AFS Transaction* **98** (1992) 308.
6. Y. SUN, H. TSAI and D. ASKELAND, *ibid.* **104** (1996) 271.
7. L. WANG, S. SHIVKUMAR and D. APELIAN, *ibid.* **181** (1990) 923.
8. J. ZHU, I. OHANKA and Y. YOSHIOKA, *J. Jpn Foundry Engng. Soc.* **72** (2000) 715.
9. J. YANG, T. HUANG and J. FU, *AFS Transaction* **128** (1998) 21.
10. Y. LIU, S. I. BAKHTIYAROV and R. A. OVERLEFT, *J. Mater. Sci.* **37** (2002) 2997.
11. I. OHNAKA, in Proceeding of the 6th International Conference on Modelling of Casting, Welding and Advance Solidification, edited by T. S. Piwonka *et al.* (MMMS, 1993) p. 337.
12. B. D. NICHOLS and C. W. HIRT, *Flow Science, inc.* Available at http://www.flow3d.com.
13. P. DAVAMI and S. M. H. MIRBAGHERI, Available at http://www.sutcast.com.
14. S. H. M. MIRBAGHERI, P. DAVAMI and N. VARAHRAM, *Intern. J. Numer. Meth. Engng.* (2002) (accepted).
15. C. M. WANG, J. PAUL and J. HUEY, in Proceeding of the 6th International Conference on Modelling of Casting, Welding and Advance Solidification, edited by T.S Piwonka *et al.* (MMMS, 1993) p. 477.
16. S. M. H. MIRBAGHERI, "Computer Simulation Fluid Flow in LFC Mould Cavity Casting by Finite Difference Method," Ph.D. Thesis, Sharif University of Technology, Iran, 2003 (In English).
17. C. W. HIRT and B. D. NICHOLS, *J. Computational Physic* **39** (1981) 201.
18. M. D. TORREY, L. D. CLOUTMAN and C. W. HIRT, "NASA-VOF2D: A Computer Program for Incompressible Flows with Free Surfaces," Technical Report LA10642-MS, Los Alamos National Laboratory, Los Alamos, New Mexico 87545 (1985).
19. M. D. TORREY, R. C. MJOLSNESS and L. R. STEIN, "NASA-VOF3D: A Three-Dimensional Computer Program for Incompressible Flow with Free Surface," Technical Report LA11009-MS, Los Alamos National Laboratory, Los Alamos, New Mexico 87545 (1987).
20. S. D. ELLIOT, "Fluid Flows Aspects of Solidification Modelling: Simulation of Low-Pressure Die-casting" Ph.D. Thesis, Queens Land University, USA, 1999.
21. S. I. BAKHTIAROV and A. OVERFELT, *AFS Transaction* **28** (2001) 271.
22. H. S. LEE, *ibid* **78** (1978) 550.

Received 26 December 2002
and accepted 5 January 2004